NASA/TM—2003-211513 AIAA–2002–0801

Gust Acoustic Response of a Single Airfoil Using the Space-Time CE/SE Method

X.Y. Wang
Taitech, Inc., Cleveland, Ohio

S.C. Chang
Glenn Research Center, Cleveland, Ohio

A. Himansu
Taitech, Inc., Cleveland, Ohio

P.C.E. Jorgenson
Glenn Research Center, Cleveland, Ohio

August 2003

The NASA STI Program Office . . . in Profile

Since its founding, NASA has been dedicated to the advancement of aeronautics and space science. The NASA Scientific and Technical Information (STI) Program Office plays a key part in helping NASA maintain this important role.

The NASA STI Program Office is operated by Langley Research Center, the Lead Center for NASA's scientific and technical information. The NASA STI Program Office provides access to the NASA STI Database, the largest collection of aeronautical and space science STI in the world. The Program Office is also NASA's institutional mechanism for disseminating the results of its research and development activities. These results are published by NASA in the NASA STI Report Series, which includes the following report types:

- TECHNICAL PUBLICATION. Reports of completed research or a major significant phase of research that present the results of NASA programs and include extensive data or theoretical analysis. Includes compilations of significant scientific and technical data and information deemed to be of continuing reference value. NASA's counterpart of peer-reviewed formal professional papers but has less stringent limitations on manuscript length and extent of graphic presentations.

- TECHNICAL MEMORANDUM. Scientific and technical findings that are preliminary or of specialized interest, e.g., quick release reports, working papers, and bibliographies that contain minimal annotation. Does not contain extensive analysis.

- CONTRACTOR REPORT. Scientific and technical findings by NASA-sponsored contractors and grantees.

- CONFERENCE PUBLICATION. Collected papers from scientific and technical conferences, symposia, seminars, or other meetings sponsored or cosponsored by NASA.

- SPECIAL PUBLICATION. Scientific, technical, or historical information from NASA programs, projects, and missions, often concerned with subjects having substantial public interest.

- TECHNICAL TRANSLATION. English-language translations of foreign scientific and technical material pertinent to NASA's mission.

Specialized services that complement the STI Program Office's diverse offerings include creating custom thesauri, building customized data bases, organizing and publishing research results . . . even providing videos.

For more information about the NASA STI Program Office, see the following:

- Access the NASA STI Program Home Page at ***http://www.sti.nasa.gov***

- E-mail your question via the Internet to help@sti.nasa.gov

- Fax your question to the NASA Access Help Desk at 301–621–0134

- Telephone the NASA Access Help Desk at 301–621–0390

- Write to:
  NASA Access Help Desk
  NASA Center for AeroSpace Information
  7121 Standard Drive
  Hanover, MD 21076

NASA/TM—2003-211513 AIAA–2002–0801

Gust Acoustic Response of a Single Airfoil Using the Space-Time CE/SE Method

X.Y. Wang
Taitech, Inc., Cleveland, Ohio

S.C. Chang
Glenn Research Center, Cleveland, Ohio

A. Himansu
Taitech, Inc., Cleveland, Ohio

P.C.E. Jorgenson
Glenn Research Center, Cleveland, Ohio

Prepared for the
40th Aerospace Sciences Meeting and Exhibit
sponsored by the American Institute of Aeronautics and Astronautics
Reno, Nevada, January 14–17, 2002

National Aeronautics and
Space Administration

Glenn Research Center

August 2003

Acknowledgments

This work was supported by NASA Glenn Research Center through contract NAS3–97186. Dr. James Scott was the Technical Monitor. X.Y. Wang would like to thank Dr. Ray Hixon for his great help in this work, Dr. James Scott for providing the GUST3D solutions, and Dr. David Kopriva for providing the DSEM solutions.

The Aerospace Propulsion and Power Program at
NASA Glenn Research Center sponsored this work.

Available from

NASA Center for Aerospace Information
7121 Standard Drive
Hanover, MD 21076

National Technical Information Service
5285 Port Royal Road
Springfield, VA 22100

Available electronically at http://gltrs.grc.nasa.gov/GLTRS

GUST ACOUSTIC RESPONSE OF A SINGLE AIRFOIL USING THE SPACE-TIME CE/SE METHOD

X.Y. Wang*
Taitech, Inc.
Cleveland, Ohio 44135

S.C. Chang†
Glenn Research Center
Cleveland, Ohio 44135

A. Himansu‡
Taitech, Inc.
Cleveland, Ohio 44135

P.C.E. Jorgenson§
Glenn Research Center
Cleveland, Ohio 44135

Abstract

A 2D parallel Euler code based on the space-time conservation element and solution element (CE/SE) method is validated by solving the benchmark problem 1 in Category 3 of the Third CAA Workshop [1]. This problem concerns the acoustic field generated by the interaction of a convected harmonic vortical gust with a single airfoil. Three gust frequencies, two gust configurations, and three airfoil geometries are considered. Numerical results at both near and far fields are presented and compared with the analytical solutions, a frequency-domain solver GUST3D solutions, and a time-domain high-order Discontinuous Spectral Element Method (DSEM) solutions. It is shown that the CE/SE solutions agree well with the GUST3D solution for the lowest frequency, while there are discrepancies between CE/SE and GUST3D solutions for higher frequencies. However, the CE/SE solution is in good agreement with the DSEM solution for these higher frequencies. It demonstrates that the CE/SE method can produce accurate results of CAA problems involving complex geometries by using unstructured meshes.

1. Introduction

The noise generated by the interaction of vortical disturbances originating upstream with propellers or turbomachinery blades has been of great interest in noise studies. A model problem regarding a two-dimensional vortical wave interaction with a single airfoil was posed as a benchmark problem in Category 3 of the Third CAA Workshop [1]. This problem involves complex geometries and flow phenomena including vorticity shedding and acoustics radiation. It has been solved by using frequency-domain solvers [2] and high-order accurate time-domain methods that solves the full nonlinear Euler equations [3,4,5].

In this paper, this problem is solved numerically by solving the unsteady 2D Euler equations using the space-time conservation element and solution element (CE/SE) method [6,7]. The CE/SE method was originally developed by Chang in 1991 [8]. It applies flux conservation to finite space-time volumes, and achieves second-order accuracy in both space and time for uniform space-time meshes. Its salient properties are summarized briefly as follows. First, both local and global flux conservations are enforced in space and time instead of in space only. Second, all the dependent variables and their spatial derivatives are considered as individual unknowns to be solved for simultaneously at each grid point. Third, every CE/SE scheme is based upon a non-dissipative scheme with addition of fully controllable numerical dissipation. This results in very low numerical dissipation. Fourth, the flux-based specification of the CE/SE schemes gives rise in a natural fashion to a simple yet generally effective non-reflecting boundary condition, which is an important issue in CAA. Some practical advantages of the CE/SE method over the high order finite difference methods are summarized as follows: 1) it can use both structured and unstructured meshes in one single algorithm to handle complex geometries, 2) it can avoid singular points without using any special treatment, and 3) it has the most compact stencil, this leads to efficient parallel computing and easy implementation of boundary conditions.

A detailed description of this method, and accompanying analysis, can be found in [6–11]. Applications of this method to CAA problems reveal that, on mesh sizes used in practice, the result is comparable to those obtained using high order compact difference schemes, even though the current solver is only 2nd-order accurate [12-18].

In this paper, a version of the 2D CE/SE Euler code that is adapted for parallel computing, is used to compute the acoustic field generated by the interaction of a vortical gust with a single airfoil. Three gust frequencies, two gust configurations, and three

*Research Engineer, Member AIAA
email: wangxy@turbot.grc.nasa.gov
†Aerospace Engineer, Member AIAA
‡Research Engineer, Member AIAA
§Aerospace Engineer, Member AIAA

airfoil geometries are considered. Numerical results at both near and far fields are presented and compared with the analytical or GUST3D or DSEM solutions.

In the following, the description of the benchmark problem is given first, which is followed by the solution procedure, initial and boundary conditions, numerical results and conclusions.

2. Problem Description

Consider a Joukowski airfoil or a flat plate with chord length c. The mean flow parameters at infinity are x-velocity U_∞, y-velocity $V_\infty = 0$, mass density ρ_∞, static pressure p_∞, and Mach number $M_\infty = 0.5$. Flow variables are non-dimensionalized by using U_∞, $c/2$, $c/(2U_\infty)$, ρ_∞ and $\rho_\infty U_\infty^2$ as the velocity, length, time, density and pressure scales, respectively [1]. As a result, the non-dimensionalized mean flow parameters at infinity are:

$$\overline{u}_\infty = 1, \ \overline{v}_\infty = 0, \quad \overline{\rho}_\infty = 1, \ \overline{p}_\infty = 1/(\gamma M_\infty^2) \quad (1)$$

Here a perfect gas with the specific heat ratio $\gamma = 1.4$ is assumed. In this paper, we will consider the steady-state Euler mean flow solution with its non-dimensionalized x-velocity $\overline{u}$, y-velocity $\overline{v}$, mass density $\overline{\rho}$ and static pressure $\overline{p}$ satisfying the following boundary conditions at infinity:

$$\overline{u} = \overline{u}_\infty, \ \overline{v} = \overline{v}_\infty, \ \overline{\rho} = \overline{\rho}_\infty, \ \overline{p} = \overline{p}_\infty \text{ (at infinity)} \quad (2)$$

Also, we will consider the unsteady Euler flow solution with its non-dimensionalized x-velocity u, y-velocity v, mass density ρ and static pressure p satisfying the following boundary conditions at infinity:

$$u = \overline{u}_\infty + u', \ v = \overline{v}_\infty + v',$$

$$\rho = \overline{\rho}_\infty + \rho', \ p = \overline{p}_\infty + p' \text{ (at infinity)} \quad (3)$$

where

$$u' \stackrel{\text{def}}{=} -(v_g \, k_y/|\mathbf{k}|)\cos(k_x x + k_y y - \omega t) \quad (4)$$

$$v' \stackrel{\text{def}}{=} (v_g \, k_x/|\mathbf{k}|)\cos(k_x x + k_y y - \omega t) \quad (5)$$

and

$$\rho' \stackrel{\text{def}}{=} 0 \quad \text{and} \quad p' \stackrel{\text{def}}{=} 0 \quad (6)$$

In Eqs. (4) and (5), (i) v_g, k_x and k_y are given constants; (ii) $|\mathbf{k}|$ is the absolute value of $\mathbf{k} = (k_x, k_y)$, i.e.,

$$|\mathbf{k}| \stackrel{\text{def}}{=} \sqrt{k_x^2 + k_y^2} \quad (7a)$$

and (iii)

$$\omega = \overline{u}_\infty k_x \quad (7b)$$

Note that Eqs. (4), (5), (7a) and (7b) imply that

$$\frac{\partial u'}{\partial x} + \frac{\partial v'}{\partial y} = 0, \quad \frac{\partial u'}{\partial t} + \frac{\partial u'}{\partial x} = 0, \quad \text{and} \quad \frac{\partial v'}{\partial t} + \frac{\partial v'}{\partial x} = 0 \quad (8)$$

As a result, (u', v', ρ', p') (which represents the undistorted gust) is a plane-wave solution to the linearized Euler equations in which $(\overline{u}_\infty, \overline{v}_\infty, \overline{\rho}_\infty, \overline{p}_\infty)$ is the constant unperturbed solution. However, because the steady-state solution $(\overline{u}, \overline{v}, \overline{\rho}, \overline{p})$ may vary in space, generally (u', v', ρ', p') is not a solution to the linearized Euler equations in which $(\overline{u}, \overline{v}, \overline{\rho}, \overline{p})$ is the unperturbed solution. In the following numerical simulations, both 1D and 2D gusts are considered. For the case of 1D gust, it is assumed that

$$v_g = 0.02, \quad k_x = 0.1, 1.0, 3.0, \quad \text{and} \quad k_y = 0 \quad (9)$$

On the other hand, for the case of 2D gust, it is assumed that

$$v_g = 0.02, \quad \text{and} \quad k_x = k_y = 0.1, 1.0, 3.0 \quad (10)$$

3. Solution Procedure

The unsteady solution (u, v, ρ, p) referred to in Sec. 2 satisfies the following 2D Euler equations:

$$\frac{\partial u_m}{\partial t} + \frac{\partial f_m}{\partial x} + \frac{\partial g_m}{\partial y} = 0, \qquad m = 1, 2, 3, 4 \quad (11)$$

Here

$$u_1 = \rho, \quad u_2 = \rho u, \quad u_3 = \rho v, \quad u_4 = E_t \quad (12)$$

$$f_1 = \rho u, \ f_2 = \rho u^2 + p, \ f_3 = \rho uv, \ f_4 = (E_t + p)u \quad (13)$$

$$g_1 = \rho v, \ g_2 = \rho uv, \ g_3 = \rho v^2 + p, \ g_4 = (E_t + p)v \quad (14)$$

with $E_t = p/(\gamma - 1) + \rho(u^2 + v^2)/2$. To proceed, let

$$u^* \stackrel{\text{def}}{=} u - \overline{u} - u', \quad v^* \stackrel{\text{def}}{=} v - \overline{v} - v',$$

$$\rho^* \stackrel{\text{def}}{=} \rho - \overline{\rho} - \rho', \quad p^* \stackrel{\text{def}}{=} p - \overline{p} - p' \quad (15)$$

and

$$\hat{u} \stackrel{\text{def}}{=} \overline{u} + u^*, \ \hat{v} \stackrel{\text{def}}{=} \overline{v} + v^*, \ \hat{\rho} \stackrel{\text{def}}{=} \overline{\rho} + \rho^*, \ \hat{p} \stackrel{\text{def}}{=} \overline{p} + p^* \quad (16)$$

Because $(\overline{u}, \overline{v}, \overline{\rho}, \overline{p})$ and (u', v', ρ', p'), respectively, represent the steady-state solution and the undistorted gust, Eq. (15) implies that (u^*, v^*, ρ^*, p^*) represents the contribution to the unsteady solution due to the presence of acoustic waves and "gust distortion". Moreover, because Eqs. (15) and (16) imply that

$$u = \hat{u} + u', \ v = \hat{v} + v', \ \rho = \hat{\rho} + \rho', \ p = \hat{p} + p' \quad (17)$$

with the aid of Eq. (3), it can be shown that, at infinity,

$$\hat{u} = \overline{u}_\infty,\ \hat{v} = \overline{v}_\infty,\ \hat{\rho} = \overline{\rho}_\infty,\ \hat{p} = \overline{p}_\infty \quad \text{(at infinity)} \tag{18}$$

Next, for each $m = 1, 2, 3, 4$, let (i) $\hat{u}_m$, $\hat{f}_m$ and $\hat{g}_m$ be the values of u_m, f_m and g_m, respectively, when u, v, ρ and p assume the values of $\hat{u}$, $\hat{v}$, $\hat{\rho}$ and $\hat{p}$, respectively, and (ii) $\overline{u}_m$, $\overline{f}_m$ and $\overline{g}_m$ be the values of u_m, f_m and g_m, respectively, when u, v, ρ and p assume the values of $\overline{u}$, $\overline{v}$, $\overline{\rho}$ and $\overline{p}$, respectively. Then because $(\overline{u}, \overline{v}, \overline{\rho}, \overline{p})$ represents the steady-state solution, one has

$$\frac{\partial \overline{u}_m}{\partial t} = 0, \quad \text{and} \quad \frac{\partial \overline{f}_m}{\partial x} + \frac{\partial \overline{g}_m}{\partial y} = 0 \tag{19}$$

Moreover, let

$$s_1 \stackrel{\text{def}}{=} u' \frac{\partial \overline{u}_1}{\partial x} + v' \frac{\partial \overline{u}_1}{\partial y} \tag{20}$$

$$s_2 \stackrel{\text{def}}{=} u' \frac{\partial \overline{u}_2}{\partial x} + v' \frac{\partial \overline{u}_2}{\partial y} + \overline{u}_1 \frac{Du'}{\partial t} \tag{21}$$

$$s_3 \stackrel{\text{def}}{=} u' \frac{\partial \overline{u}_3}{\partial x} + v' \frac{\partial \overline{u}_3}{\partial y} + \overline{u}_1 \frac{Dv'}{\partial t} \tag{22}$$

$$s_4 \stackrel{\text{def}}{=} u' \frac{\partial \overline{u}_4}{\partial x} + v' \frac{\partial \overline{u}_4}{\partial y} + \overline{u}_2 \frac{Du'}{\partial t} + \overline{u}_3 \frac{Dv'}{\partial t} \tag{23}$$

with

$$\frac{Du'}{\partial t} \stackrel{\text{def}}{=} \frac{\partial u'}{\partial t} + \overline{u} \frac{\partial u'}{\partial x} + \overline{v} \frac{\partial u'}{\partial y} \tag{24}$$

and

$$\frac{Dv'}{\partial t} \stackrel{\text{def}}{=} \frac{\partial v'}{\partial t} + \overline{u} \frac{\partial v'}{\partial x} + \overline{v} \frac{\partial v'}{\partial y} \tag{25}$$

Then Eqs. (8), (12)–(17) and (19), and the fact that (u', v', ρ', p') and (u^*, v^*, ρ^*, p^*) are small perturbations of $(\overline{u}, \overline{v}, \overline{\rho}, \overline{p})$ (Note: $v_g \ll 1$) imply that the relation

$$\frac{\partial u_m}{\partial t} + \frac{\partial f_m}{\partial x} + \frac{\partial g_m}{\partial y} = \frac{\partial \hat{u}_m}{\partial t} + \frac{\partial \hat{f}_m}{\partial x} + \frac{\partial \hat{g}_m}{\partial y} + s_m \tag{26}$$

where $m = 1, 2, 3, 4$, is accurate to the first order in v_g. Combining Eqs. (11) and (26), one has

$$\frac{\partial \hat{u}_m}{\partial t} + \frac{\partial \hat{f}_m}{\partial x} + \frac{\partial \hat{g}_m}{\partial y} = -s_m, \quad m = 1, 2, 3, 4 \tag{27}$$

The current numerical simulation includes the following steps: (i) evaluation of the steady-state solution $\overline{u}_m$ (or equivalently $(\overline{u}, \overline{v}, \overline{\rho}, \overline{p})$); (ii) evaluation of s_m using Eqs. (4), (5) and (20)–(23); (iii) evaluation of $\hat{u}_m$ (or equivalently $(\hat{u}, \hat{v}, \hat{\rho}, \hat{p})$) using Eq. (27); and (iv) evaluation of (u^*, v^*, ρ^*, p^*) using Eq. (16). Note that, (i) because the convective distortion of the gust generates no acoustic waves, p^* represents the acoustic pressure generated by the interaction of the gust with the airfoil, and (ii) the solved problem is linear, therefore its solution can be superimposed.

4. Initial and Boundary Conditions

Here we specify the numerical initial and boundary conditions applied when solving Eq. (27) for $\hat{u}_m$. At $t = 0$, the marching variables are specified using the steady-state solution. Moreover, at any point on the airfoil surface, it is assumed that the velocity (u, v) is tangent to the airfoil. By using Eq. (17), this implies that

$$n_x \hat{u} + n_y \hat{v} = -(n_x u' + n_y v') \tag{28}$$

where (n_x, n_y) is any unit vector normal to the airfoil at the point under consideration.

On the other hand, at any spatial mesh point on the outer boundary of the computational domain, the values of u_m^*, u_{mx}^* and u_{my}^* at the nth time level, respectively, are specified using the $(n - 1/2)$th time level value of the corresponding variables at the interior spatial point immediately neighboring to it. It has been shown numerically that these boundary condition are non-reflecting in nature [7].

5. Numerical Results

In the following, numerical results will be presented for two gust configurations, three gust frequencies, and three airfoil geometries. A 2D parallel CE/SE Euler solver, with no slope-limiting ($\alpha = 0$) and with added-numerical-dissipation ($\epsilon = 0.5$)[9], is used in the computation. The numerical solution of the acoustic pressure non-dimensionalized by v_g is plotted in all figures. The RMS pressure on the airfoil surface, and the sound intensity at one and four chord lengths from the origin, are presented for all cases to examine both the near and far field solutions.

5.1 Flat-Plate Airfoil

For this case, the analytical and numerical solutions are independent of k_y. The obtained solutions are plotted in Figs. 1–3 for $k_x = 0.1, 1.0$, and 3.0, respectively. It can be seen that a fairly good agreement with the analytical solution is achieved for both low and high frequencies. For $k_x = 1.0$, the CE/SE solution is slightly different from the analytical solution.

As an example, for the case $k_x = 3.0$, a computational domain of $-23 \leq x, y \leq 23$ with 921x921 uniformly distributed mesh points is used. The total number of triangular cells is 846400 and $\Delta t =$

$T/120$, with $T = 2\pi/\omega$ being the time period of the gust. The solutions settle into a time-periodic pattern by $t = 15T$(3600 marching steps). Note that, for the CE/SE method, a time period of $\Delta t/2$ is advanced by each marching step. The computation takes 0.5 hours walltime using 32 CPUs on SGI Origin 2000 system with 250 MHz MIPS R10000 processors.

5.2 Symmetric Airfoil

The symmetric Joukowski airfoil of 12% thickness is considered here. As shown in Fig. 4, the airfoil is surrounded by an unstructured mesh (Fig. 4(a)) which, in turn, is embedded in a structured mesh (Fig. 4(b)). The unstructured mesh is generated by using TRUMPET [19]. The mean pressure on the airfoil surface is plotted in Fig. 5 and compared with the potential code FLO36 solutions. The corresponding acoustic solutions are shown in Figs. 6–8 for the 2D gust case at different frequencies. A reasonable agreement between CE/SE and GUST3D solutions is observed for $k_x = k_y = 0.1$, while there are large discrepancies for $k_x = k_y = 1.0$ and 3.0. However, the CE/SE solutions agree well with the DSEM solution for $k_x = k_y = 1.0$ and 3.0. In Figs. 9–11, the computed solutions for the 1D gust case are shown for different frequencies. For $k_x = 0.1$ and 1.0, the CE/SE solutions agree well with the GUST3D solution in the near field and have slight differences in the far field.

Note that, for the symmetric airfoil case, the DSEM results given in [5] do not provide (i) any 2D gust solutions with $k_x = k_y = 0.1$; (ii) the sound intensity at one chord length due to the 2D gust with either $k_x = k_y = 1.0$ or $k_x = k_y = 3.0$; and (iii) any 1D gust solutions. Also note that no GUST3D solutions are available for the 1D gust case with $k_x = 3.0$ and $k_y = 0$, and the 2D gust case with $k_x = k_y = 3.0$.

As an example, a computational domain of $-23 \leq x, y \leq 23$ is used for $k_x = k_y = 3.0$. An unstructured mesh with 7392 triangles is used in the region of $-2 \leq x, y \leq 2$ while a uniform structured mesh formed from 420000 triangles is used in the rest of the computational domain. The RMS pressure solution converges by $t = 10T$ (14000 marching steps). The computation takes 1.5 hours walltime using 16 CPUs on SGI Origin 2000 system with 400 MHz MIPS R12000 processors.

5.3 Cambered Airfoil

The airfoil considered here has the same thickness as the symmetric airfoil but with a camber ratio of 0.02 and an angle of attack of 2°. The steady lift is no longer zero and the flow field is more complex. A larger computational domain is necessary. As an example, a computational domain of $-40 \leq x, y \leq 40$ is used for the case $k_x = k_y = 1.0$. Among the 643744 triangular cells that fill the entire computational domain, 5344 cells are contained in the region of $-2 \leq x, y \leq 2$ (see Fig. 12). The numerical results are obtained assuming $\Delta t = T/1050$.

The computed mean pressure on the airfoil surface is plotted in Fig. 13 with the FLO36 solution, showing that the CE/SE solution on the upper surface is slightly under-predictive. For the two frequencies $k_x = 0.1$ and 1.0, the unsteady solutions are plotted in Figs. 14–15 for the 2D gust case and in Figs. 16–17 for the 1D gust case, respectively. The CE/SE solutions are very close to the GUST3D solution for both 1D gust case and 2D gust case at $k_x = 0.1$. However larger discrepancies are observed for $k_x = 1.0$. The CE/SE solution is very similar to the DSEM solution for the 2D gust case at $k_x = 1.0$.

The domain size study is performed for the cambered airfoil for the 2D gust case at $k_x = 1.0$. The near field solutions, including the RMS pressure on the airfoil surface and the sound intensity at one chord length, obtained in a smaller domain of $-23 \leq x, y \leq 23$, are identical to the solution presented above. The sound intensity at four chord lengths is slightly different from the presented solution. The non-reflecting boundary condition has some reflections that are generated at the far-field boundary, which is also observed in the RMS pressure contour plot. However the reflection is generally less than 5% of the maximum value of the acoustic field and has little effect on the accuracy of the numerical solutions.

Grid refinement study is not performed because the mesh used in the computation is fine enough to capture both the acoustic waves and the gust. About 30–40 mesh points per wave length are necessary for the CE/SE method since it is 2nd order accurate. In the current computation, about 40 mesh points per wave length are used.

6. Conclusions

The 2D parallel CE/SE Euler code has been used to solve the Problem 1 in Category 3 of the Third CAA Workshop. Three gust frequencies, two gust configurations, and three airfoil geometries have been studied. A fairly good agreement between the CE/SE and GUST3D solutions in both near and far fields is achieved for the lowest frequency. There are some discrepancies between CE/SE and GUST3D solutions for higher frequencies. However, the CE/SE solution is in good agreement with the DSEM solution for these higher frequencies. It

is concluded that the CE/SE method can produce accurate solution with a simple and general non-reflecting boundary condition. No special treatment is needed for the singular geometric boundary points, such as the leading edge point of the flat-plate airfoil and the trailing edge point of the symmetric and cambered airfoils. The CE/SE method can handle the complex geometry well by using the unstructured mesh. This work demonstrates that the CE/SE method is capable of producing accurate solutions of CAA problems involving complex geometries.

Acknowledgments

This work was supported by NASA Glenn Research Center through Contract NAS3-97186. Dr. James Scott is the Technical Monitor. The first author would like to thank Dr. Ray Hixon for his great help in this work, Dr. James Scott for providing the GUST3D solutions, and Dr. David Kopriva for providing the DSEM solutions.

7. References

[1] The Proceeding of the Third Computational Aeroacoustics (CAA) Workshop on Benchmark Problems, NASA/CP-2000-209790, August, 2000.

[2] J.R. Scott and H.M. Atassi, "A Finite-Difference Frequency-Domain Numerical Scheme for the Solution of the Gust-Response Problem," *J. Comput. Phys.*, **119,** pp. 75-93, (1995).

[3] D.P. Lockard and P.J. Morris, "The Radiated Noise from Airfoils in Realistic Mean Flows," AIAA Paper 97-0286, January, 1997.

[4] R. Hixon, R.R. Mankbadi, and J.R. Scott, "Validation of a High-Order Prefactored Compact Code on Nonlinear Flows with Complex Geometries," AIAA Paper 2001-1103, January, 2001.

[5] P. Rasetarinera, D.A. Kopriva, and M.Y. Hussaini, "Discontinuous Spectral Element Solution of Aeroacoustic Problems," in *Proceedings of the Third Computational Aeroacoustics (CAA) Workshop on Benchmark Problems*, NASA/CP-2000-209790, pp. 103.

[6] S.C. Chang, "The Method of Space-Time Conservation Element and Solution Element – A New Approach for Solving the Navier-Stokes and Euler Equations," *J. Comput. Phys.*, **119,** pp. 295-324, (1995).

[7] S.C. Chang, X.Y. Wang, and C.Y. Chow, "The Space-Time Conservation Element and Solution Element Method – A New High-Resolution and Genuinely Multidimensional Paradigm for Solving Conservation Laws," *J. Comput. Phys.*, **156**, pp. 89–136, (1999).

[8] S.C. Chang and W.M. To, "A New Numerical Framework for Solving Conservation Laws– The Method of Space-Time Conservation Element and Solution Element," NASA TM 104495, August 1991.

[9] X.Y. Wang and S.C. Chang, "A 2D Non-splitting Unstructured-triangular-mesh Euler Solver based on the Method of Space-Time Conservation Element and Solution Element," Vol. 8, No. 2, pp. 326-340, 1999, *Computational Fluid Dynamics JOURNAL.*

[10] X.Y. Wang and S.C. Chang, "A 3D Non-splitting Structured/Unstructured Euler Solver based on the Method of Space-Time Conservation Element and Solution Element," AIAA Paper 98-3278, Norfolk, Virginia, June, 1998.

[11] A. Himansu, P. Jorgenson, X.Y. Wang and S.C. Chang, "Parallel CE/SE Computations via Domain Decomposition," in *Proceedings of 1st International Conference of Computational Fluid Dynamics*, Kyoto, June, 2000.

[12] S.C. Chang, A. Himansu, C.Y. Loh, X.Y. Wang, S.T. Yu and P.C.E. Jorgenson, "Robust and Simple Non-Reflecting Boundary Conditions for the Space-Time Conservation Element and Solution Element Method," AIAA Paper 97-2077, June 29-July 2, 1997, Snowmass, CO.

[13] C.Y. Loh, S.C. Chang, J.R. Scott and S.T. Yu, "The Space-Time Conservation Element Method – A New Numerical Scheme for Computational Aeroacoustics," AIAA Paper 96-0276, January 15-18, 1996, Reno, NV.

[14] C.Y. Loh, L.S. Hultgren and S.C. Chang, "Computing Waves in Compressible Flow Using the Space-Time Conservation Element and Solution Element method," AIAA Paper 98-0369, January 12-15, 1998, Reno, NV.

[15] X.Y. Wang, C.Y. Chow and S.C. Chang, "Numerical Simulation of Gust Generated Aeroacoustics in a Cascade Using the Space-Time Conservation Element and Solution Element

Method," AIAA Paper 98-0178, January 12-15, 1998, Reno, NV.

[16] X.Y. Wang, S.C. Chang, and P. Jorgenson, "Prediction of Sound Waves Propagating through a Nozzle without/with a Shock Wave Using the Space-Time CE/SE Method," AIAA 2000-0222, Reno, NV, January, 2000.

[17] X.Y. Wang, S.C. Chang, and P. Jorgenson, "Accuracy Study of the Space-Time CE/SE Method for Computational Aeroacoustics Problems Involving Shock Waves," AIAA 2000-0474, Reno, NV, January, 2000.

[18] X.Y. Wang, A. Himansu, P. Jorgenson, and S.C. Chang, "Gust Acoustic Response of a Swept Rectilinear Cascade Using the Space-Time CE/SE Method," FEDSM 2001-18134, in *Proceedings of FEDSM'01 2001 Fluids Engineering Summer Meeting*, May 29–June 1, 2001.

[19] P.C.E. Jorgenson and R.H. Pletcher, "An Implicit Numerical Scheme for the Simulation of Internal Viscous Flows on Unstructured Grids," AIAA-94-0306, January 1994.

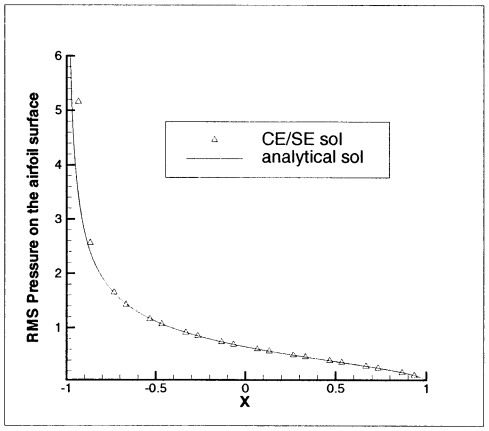

(a) RMS pressure on the flat-plate surface.

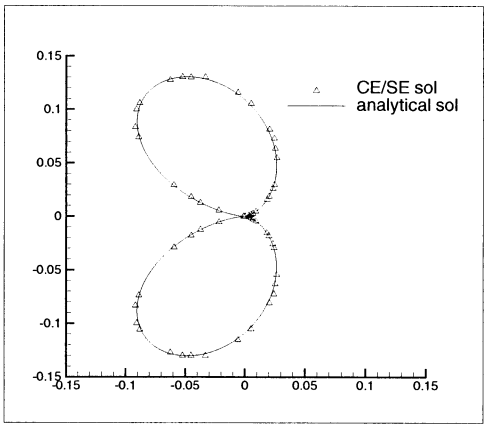

(b) Sound intensity at one chord length.

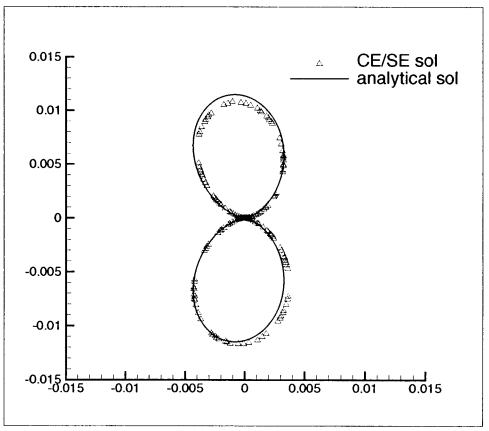

(c) Sound intensity at four chord lengths.

Figure 1: CE/SE solutions for the flat plate case assuming $k_x = 0.1$.

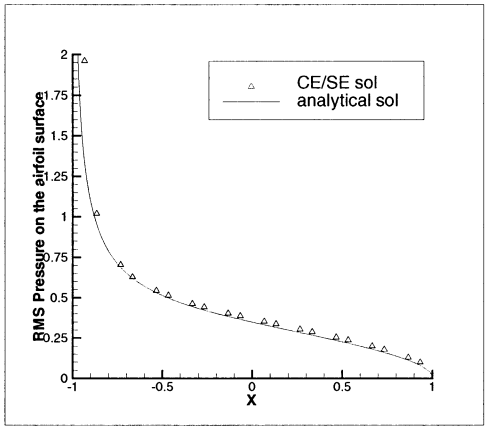

(a) RMS pressure on the flat-plate surface.

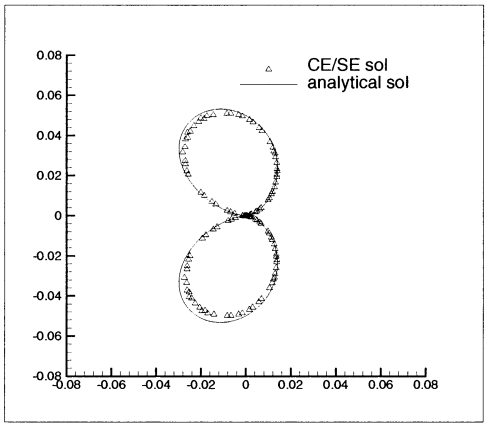

(b) Sound intensity at one chord length.

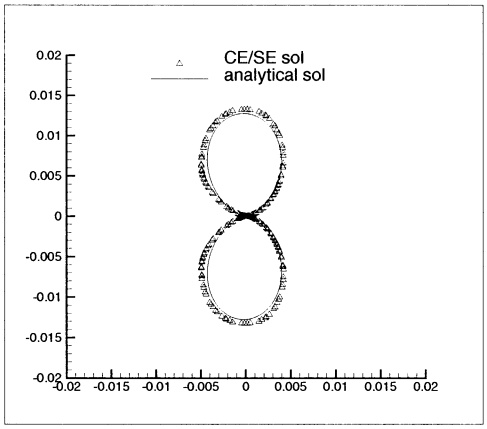

(c) Sound intensity at four chord lengths.

Figure 2: CE/SE solutions for the flat plate case assuming $k_x = 1.0$.

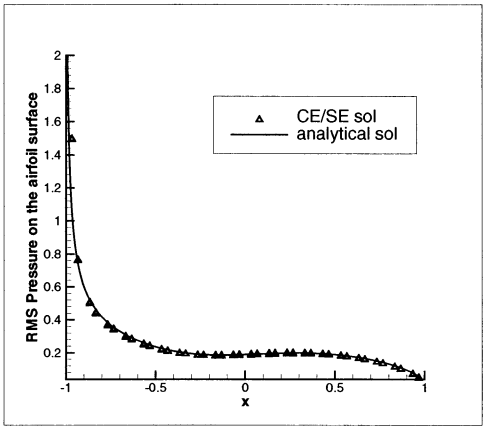

(a) RMS pressure on the flat-plate surface.

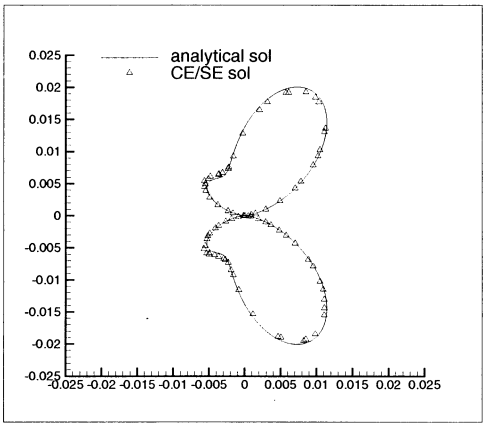

(b) Sound intensity at one chord length.

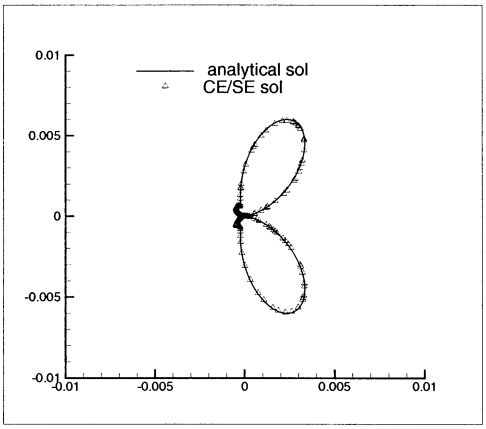

(c) Sound intensity at four chord lengths.

Figure 3: CE/SE solutions for the flat plate case assuming $k_x = 3.0$.

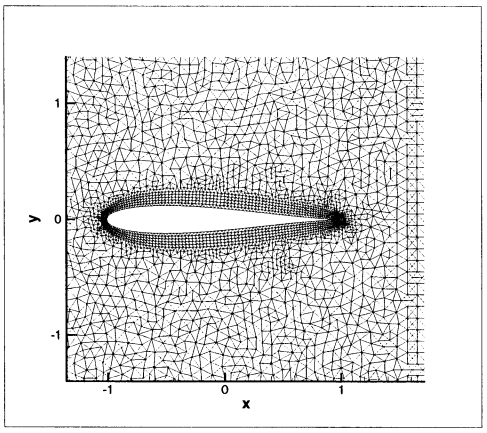

(a)

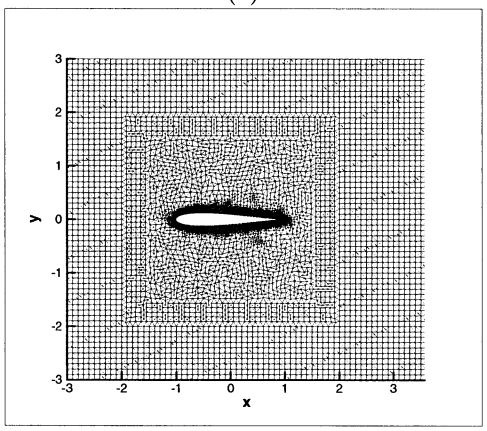

(b)

Figure 4: Structured/Unstructured mesh used for the symmetric airfoil calculation.

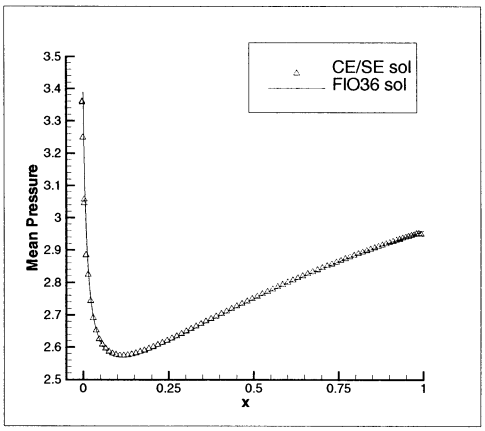

Figure 5: Mean pressure distribution on the airfoil surface for the symmetric airfoil.

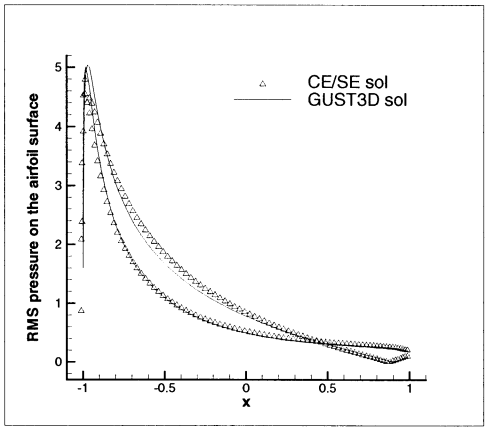

(a) RMS pressure on the airfoil surface.

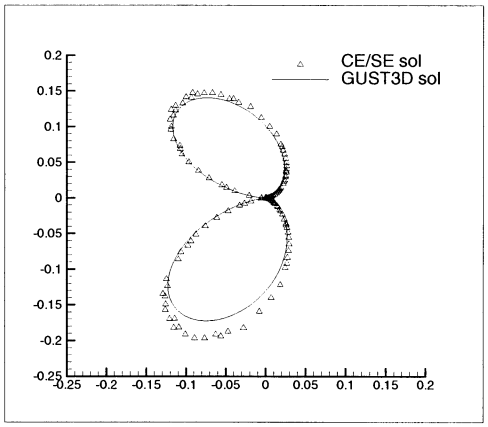

(b) Sound intensity at one chord length.

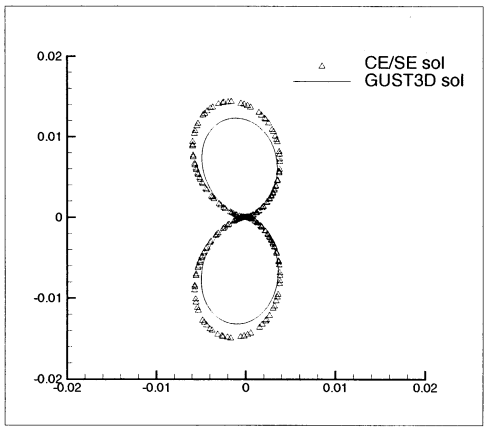

(c) Sound intensity at four chord lengths.

Figure 6: CE/SE solutions for the symmetric airfoil case assuming $k_x = k_y = 0.1$.

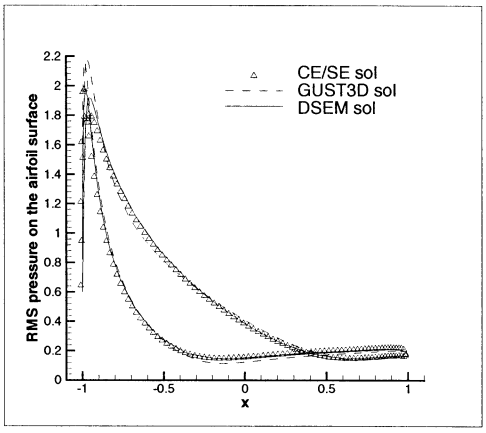

(a) RMS pressure on the airfoil surface.

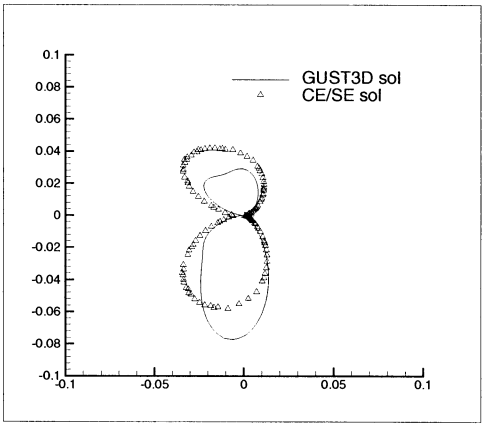

(b) Sound intensity at one chord length.

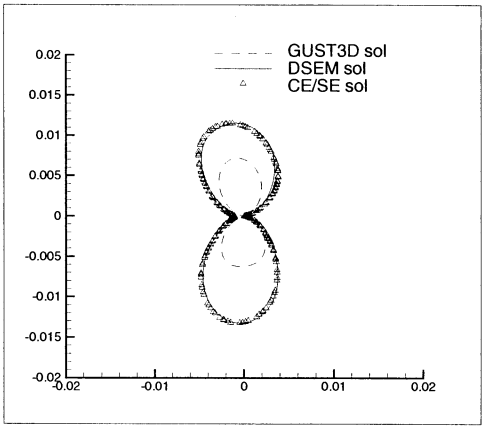

(c) Sound intensity at four chord lengths.

Figure 7: CE/SE solutions for the symmetric airfoil case assuming $k_x = k_y = 1.0$.

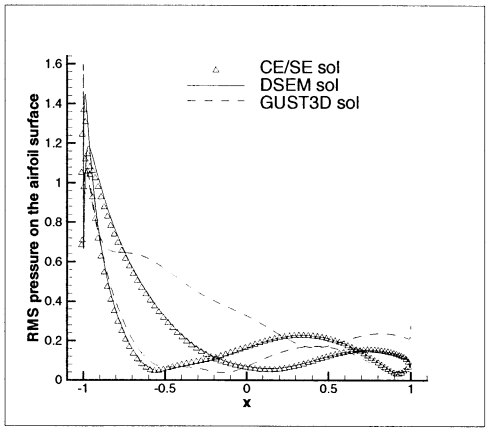

(a) RMS pressure on the airfoil surface.

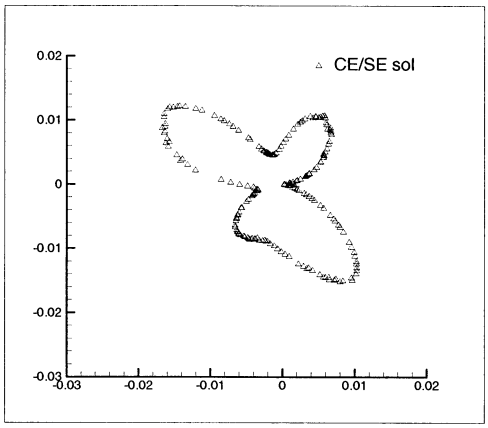

(b) Sound intensity at one chord length.

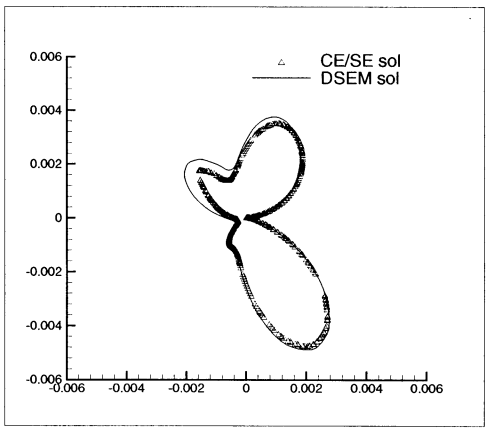

(c) Sound intensity at four chord lengths.

Figure 8: CE/SE solutions for the symmetric airfoil case assuming $k_x = k_y = 3.0$.

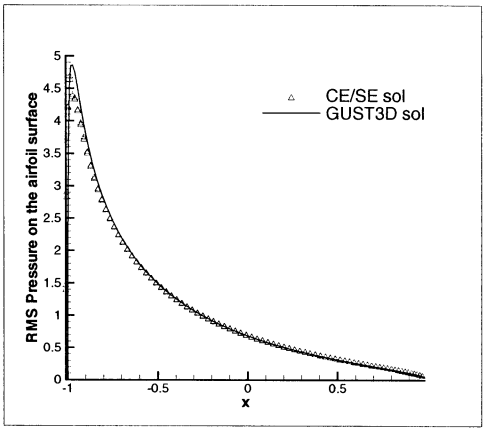

(a) RMS pressure on the airfoil surface.

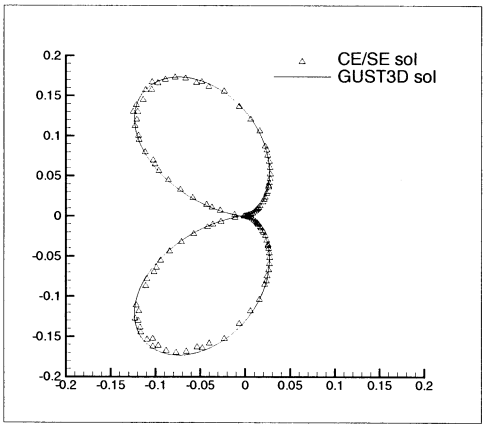

(b) Sound intensity at one chord length.

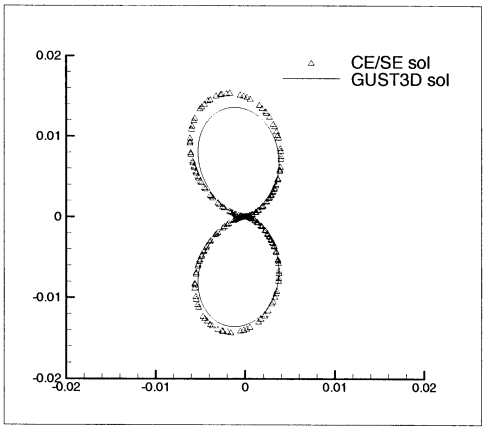

(c) Sound intensity at four chord lengths.

Figure 9: CE/SE solutions for the symmetric airfoil case assuming $k_x = 0.1, k_y = 0.0$.

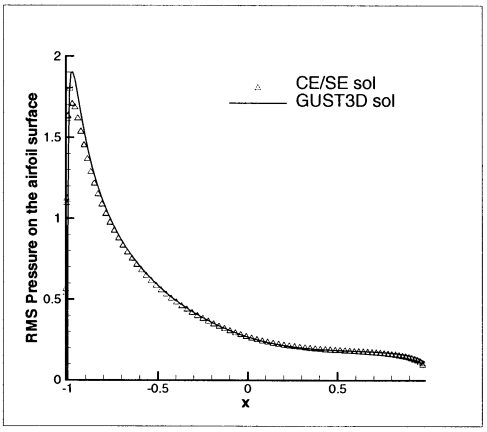

(a) RMS pressure on the airfoil surface.

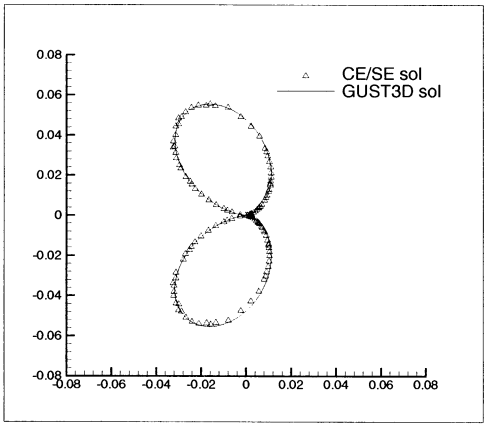

(b) Sound intensity at one chord length.

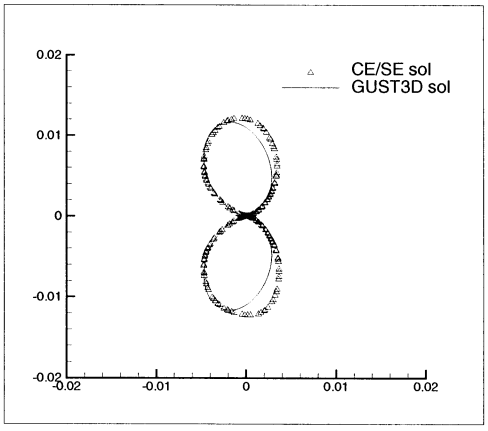

(c) Sound intensity at four chord lengths.

Figure 10: CE/SE solutions for the symmetric airfoil case assuming $k_x = 1.0, k_y = 0.0$.

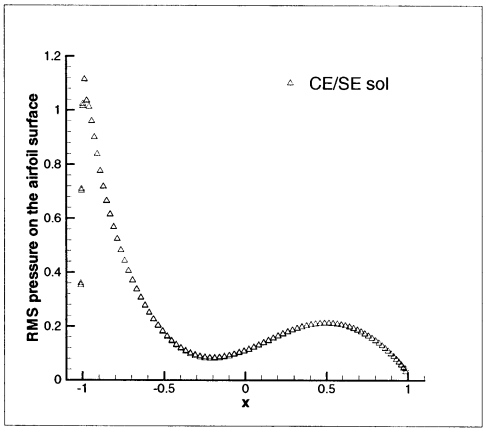

(a) RMS pressure on the airfoil surface.

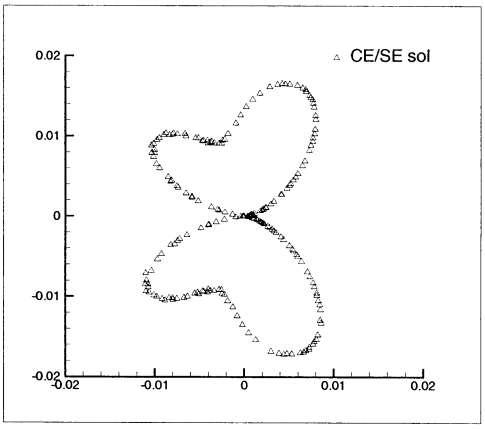

(b) Sound intensity at one chord length.

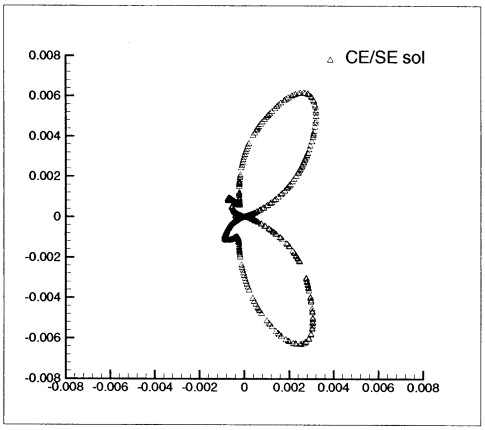

(c) Sound intensity at four chord lengths.

Figure 11: CE/SE solutions for the symmetric airfoil case assuming $k_x = 3.0, k_y = 0.0$.

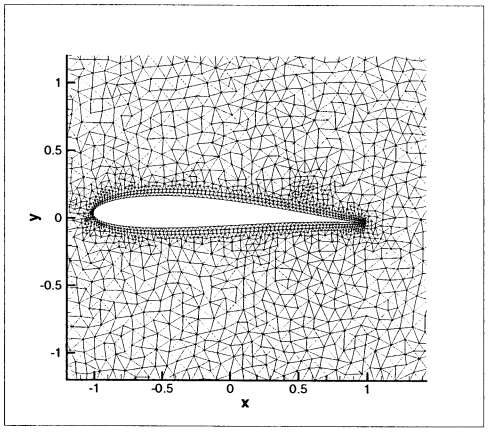

(a)

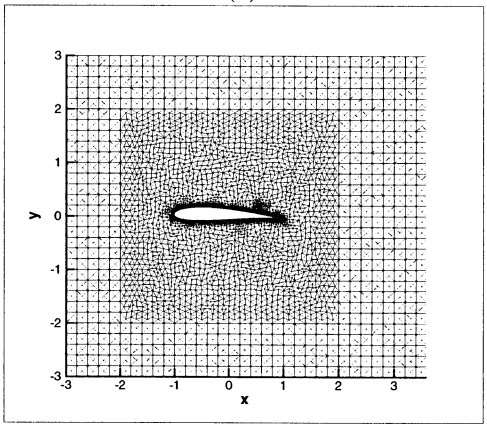

(b)

Figure 12: Structured/Unstructured mesh used in the cambered airfoil calculation.

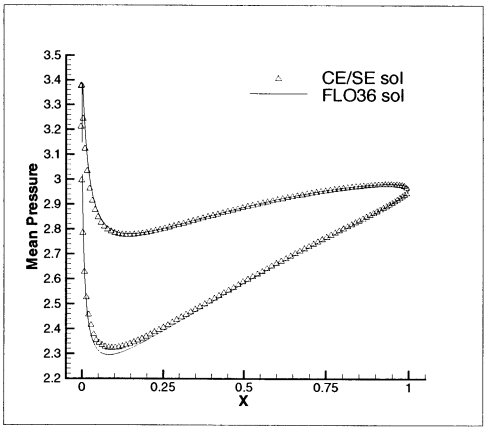

Figure 13: Mean pressure distribution on the airfoil surface for the cambered airfoil.

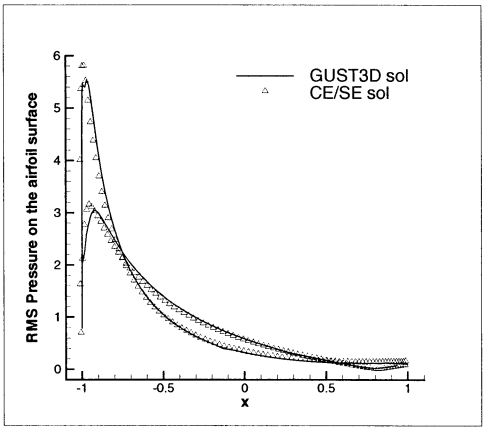

(a) RMS pressure on the airfoil surface.

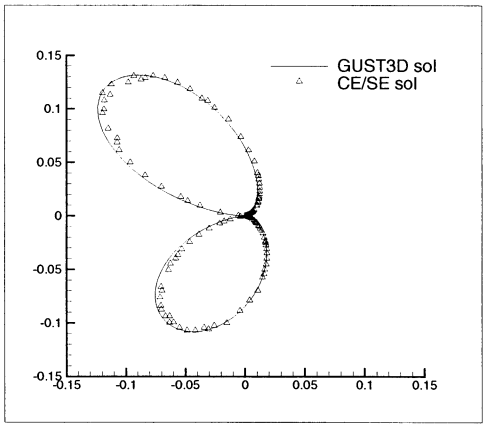

(b) Sound intensity at one chord length.

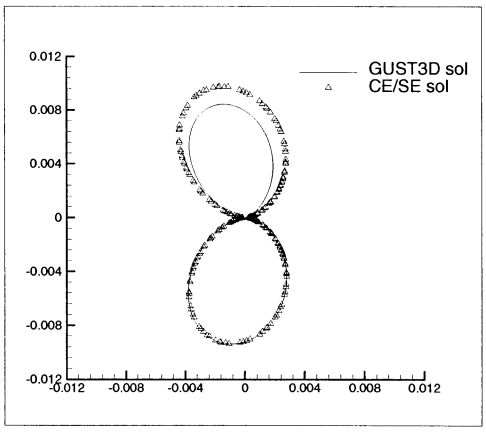

(c) Sound intensity at four chord lengths.

Figure 14: CE/SE solutions for the cambered airfoil case assuming $k_x = k_y = 0.1$.

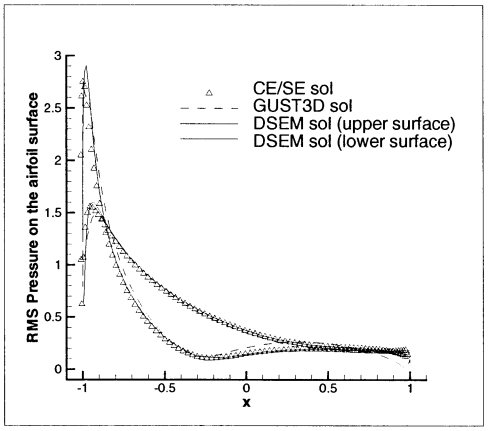

(a) RMS pressure on the airfoil surface.

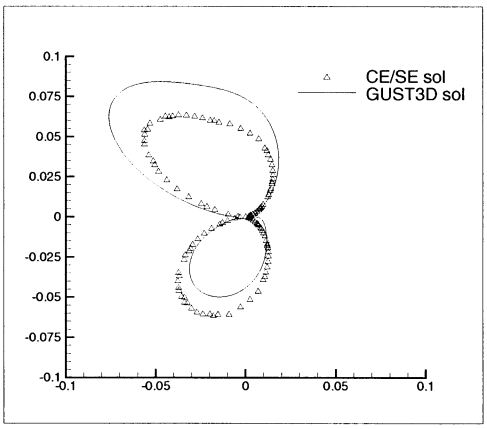

(b) Sound intensity at one chord length.

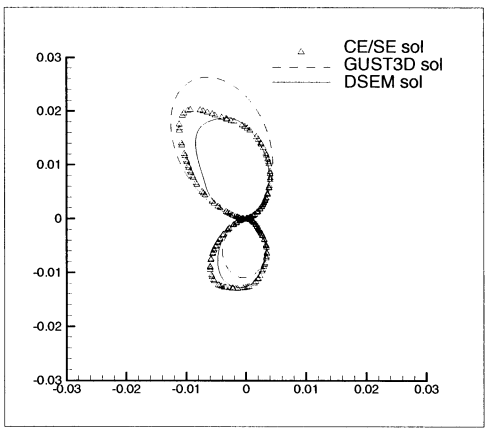

(c) Sound intensity at four chord lengths.

Figure 15: CE/SE solutions for the cambered airfoil case assuming $k_x = k_y = 1.0$.

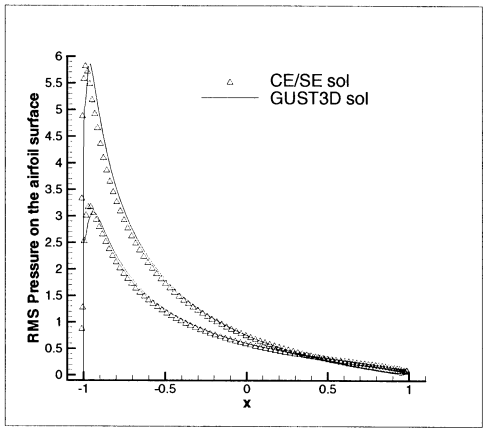

(a) RMS pressure on the airfoil surface.

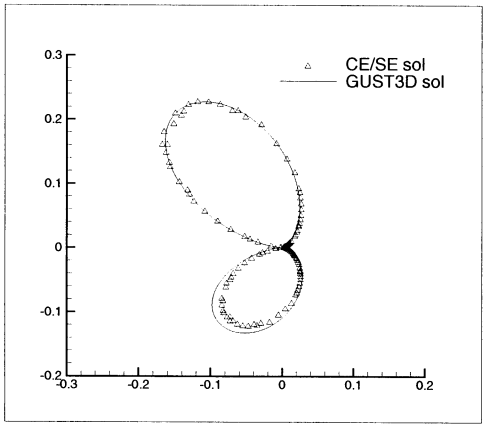

(b) Sound intensity at one chord length.

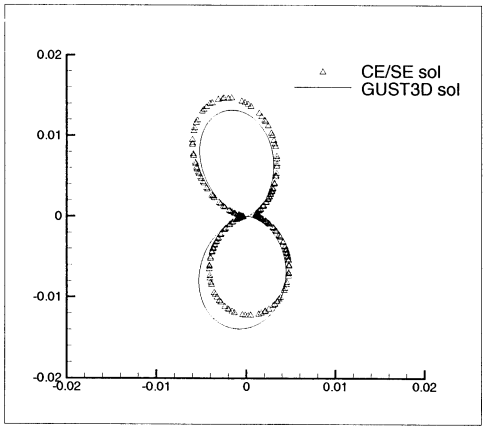

(c) Sound intensity at four chord lengths.

Figure 16: CE/SE solutions for the cambered airfoil case assuming $k_x = 0.1, k_y = 0.0$.

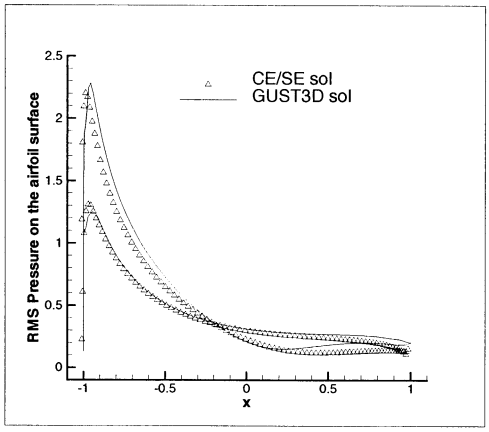

(a) RMS pressure on the airfoil surface.

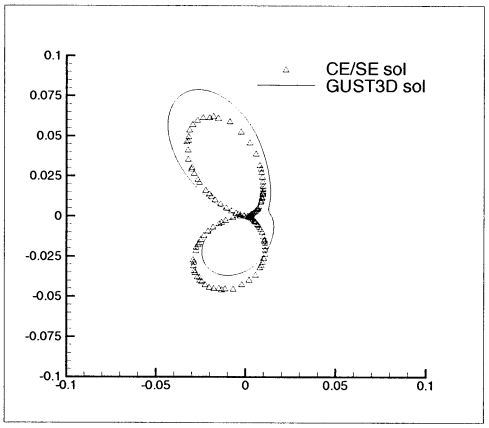

(b) Sound intensity at one chord length.

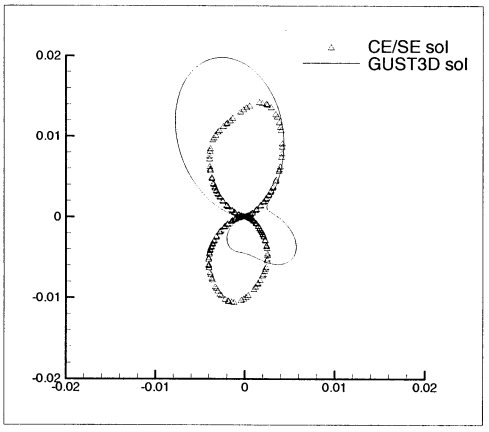

(c) Sound intensity at four chord lengths.

Figure 17: CE/SE solutions for the cambered airfoil case assuming $k_x = 1.0, k_y = 0.0$.

REPORT DOCUMENTATION PAGE

Form Approved
OMB No. 0704-0188

1. AGENCY USE ONLY (*Leave blank*)	2. REPORT DATE	3. REPORT TYPE AND DATES COVERED
	August 2003	Technical Memorandum

4. TITLE AND SUBTITLE

Gust Acoustic Response of a Single Airfoil Using the Space-Time CE/SE Method

5. FUNDING NUMBERS

WU–708–90–33–00

6. AUTHOR(S)

X.Y. Wang, S.C. Chang, A. Himansu, and P.C.E. Jorgenson

7. PERFORMING ORGANIZATION NAME(S) AND ADDRESS(ES)

National Aeronautics and Space Administration
John H. Glenn Research Center at Lewis Field
Cleveland, Ohio 44135–3191

8. PERFORMING ORGANIZATION REPORT NUMBER

E–13305

9. SPONSORING/MONITORING AGENCY NAME(S) AND ADDRESS(ES)

National Aeronautics and Space Administration
Washington, DC 20546–0001

10. SPONSORING/MONITORING AGENCY REPORT NUMBER

NASA TM—2003-211513
AIAA–2002–0801

11. SUPPLEMENTARY NOTES

Prepared for the 40th Aerospace Sciences Meeting and Exhibit sponsored by the American Institute of Aeronautics and Astronautics, Reno, Nevada, January 14–17, 2002. X.Y. Wang and A. Himansu, Taitech, Inc., Cleveland, Ohio 44135; S.C. Chang and P.C.E. Jorgenson, NASA Glenn Research Center. Responsible person, S.C. Chang, organization code 5880, 216–433–5874.

12a. DISTRIBUTION/AVAILABILITY STATEMENT

Unclassified - Unlimited
Subject Category: 34 Distribution: Nonstandard

Available electronically at http://gltrs.grc.nasa.gov/GLTRS

This publication is available from the NASA Center for AeroSpace Information, 301–621–0390.

12b. DISTRIBUTION CODE

13. ABSTRACT ***(Maximum 200 words)***

A 2D parallel Euler code based on the space-time conservation element and solution element (CE/SE) method is validated by solving the benchmark problem I in Category 3 of the Third CAA Workshop [1]. This problem concerns the acoustic field generated by the interaction of a convected harmonic vortical gust with a single airfoil. Three gust frequencies, two gust configurations, and three airfoil geometries are considered. Numerical results at both near and far fields are presented and compared with the analytical solutions, a frequency-domain solver GUST3D solutions, and a time-domain high-order Discontinuous Spectral Element Method (DSEM) solutions. It is shown that the CE/SE solutions agree well with the GUST3D solution for the lowest frequency, while there are discrepancies between CE/SE and GUST3D solutions for higher frequencies. However, the CE/SE solution is in good agreement with the DSEM solution for these higher frequencies. It demonstrates that the CE/SE method can produce accurate results of CAA problems involving complex geometries by using unstructured meshes.

14. SUBJECT TERMS

Space-time CE/SE method; Computational aeroacoustics

15. NUMBER OF PAGES

19

16. PRICE CODE

17. SECURITY CLASSIFICATION OF REPORT	18. SECURITY CLASSIFICATION OF THIS PAGE	19. SECURITY CLASSIFICATION OF ABSTRACT	20. LIMITATION OF ABSTRACT
Unclassified	Unclassified	Unclassified	